



# Crystal structure of a Y-box binding protein 1 (YB-1)–RNA complex reveals key features and residues interacting with RNA

Received for publication, February 11, 2019, and in revised form, May 26, 2019. Published, Papers in Press, June 3, 2019, DOI 10.1074/jbc.RA119.007545

Xiao-Juan Yang<sup>‡§¶</sup>, Hong Zhu<sup>‡§</sup>, Shi-Rong Mu<sup>‡§</sup>, Wen-Juan Wei<sup>‡§</sup>, Xun Yuan<sup>§¶</sup>, Meng Wang<sup>‡§</sup>, Yanchao Liu<sup>§¶</sup>, Jingyi Hui<sup>‡§¶1</sup>, and Ying Huang<sup>§¶2</sup>

From the <sup>‡</sup>CAS Center for Excellence in Molecular Cell Science, Shanghai 200031, China, the <sup>§</sup>State Key Laboratory of Molecular Biology, Shanghai Institute of Biochemistry and Cell Biology, Chinese Academy of Sciences, University of Chinese Academy of Sciences, Shanghai 200031, China, and the <sup>¶</sup>Shanghai Key Laboratory of Molecular Andrology, Shanghai 200031, China

Edited by Wolfgang Peti

The Y-box binding protein 1 (YB-1) is a member of the cold shock domain (CSD) protein family and is recognized as an oncogenic factor in several solid tumors. By binding to RNA, YB-1 participates in several steps of posttranscriptional regulation of gene expression, including mRNA splicing, stability, and translation; microRNA processing; and stress granule assembly. However, the mechanisms in YB-1-mediated regulation of RNAs are unclear. Previously, we used both systematic evolution of ligands by exponential enrichment (SELEX) and individual-nucleotide resolution UV cross-linking and immunoprecipitation coupled RNA-Seq (iCLIP-Seq) analyses, which defined the RNA-binding consensus sequence of YB-1 as CA(U/C)C. We also reported that through binding to its core motif CAUC in primary transcripts, YB-1 regulates the alternative splicing of a *CD44* variable exon and the biogenesis of miR-29b-2 during both Drosha and Dicer steps. To elucidate the molecular basis of the YB-1–RNA interactions, we report high-resolution crystal structures of the YB-1 CSD in complex with different RNA oligos at 1.7 Å resolution. The structure revealed that CSD interacts with RNA mainly through  $\pi$ – $\pi$  stacking interactions assembled by four highly conserved aromatic residues. Interestingly, YB-1 CSD forms a homodimer in solution, and we observed that two residues, Tyr-99 and Asp-105, at the dimer interface are important for YB-1 CSD dimerization. Substituting these two residues with Ala reduced CSD's RNA-binding activity and abrogated the splicing activation of YB-1 targets. The YB-1 CSD–RNA structures presented here at atomic

resolution provide mechanistic insights into gene expression regulated by CSD-containing proteins.

The Y-box binding protein 1 (YB-1) is a nucleic acid-binding protein that belongs to the highly conserved cold shock domain (CSD)<sup>3</sup>-containing protein family found in bacteria, plants, and animals (1, 2). It was originally identified by its ability to bind Y-box sequence 5'-CTGATTGGCCAA-3' (an inverted CCAAT cassette) in the promoter of the major histocompatibility complex class II gene (3). Subsequently, YB-1 was characterized as a major component of the messenger ribonucleoprotein particles in the cytoplasm that interacts with mRNAs (4). Accumulating evidence has suggested that YB-1 participates in almost all DNA- and RNA-related processes in cells, from DNA replication and repair to the transcription, splicing, stability, and translation of mRNA through its DNA/RNA-binding activities and interactions with other proteins (1, 2, 5–12). However, the underlying regulatory mechanisms remain elusive.

The biological functions of YB-1 have been extensively studied in diseases, mainly including malignant tumors (13). It has been shown that transgenic mice overexpressing YB-1 developed invasive mammary carcinomas (14). Numerous reports suggest that the up-regulation of YB-1 and its nuclear localization are indicators of poor prognosis in a variety of cancers (15, 16). YB-1 plays crucial roles in the control of multiple cellular processes, including cell proliferation, survival, metastasis, and drug resistance. It regulates the transcription of genes involved in drug resistance and the control of cell proliferation and progression, including *MDR1* (17), *CCNA* and *CCNB1* (18), *EGFR* (19), *PIK3C* (20), *MET* (21), and *CD44* (22). YB-1 has also been shown to act as a critical regulator of translation during the epithelial–mesenchymal transition and metastasis of epithelial malignancies by activating the translation of Snail1, HIF1A, and other developmentally regulated factors (23, 24). In addition,

This work was supported by National Natural Science Foundation of China Grants 91640102 and 31870741 (to Y. H.) and 31570820, 31661143035, and 31770881 (to J. H.), National Key Research and Development Program of China Grant 2017YFA0504400 (to J. H.), Strategic Priority Research Program of the Chinese Academy of Sciences Grants XDB08010202 (to Y. H.) and XDB19000000 (to J. H.), the Chinese Academy of Sciences Facility-based Open Research Program, and the State Key Laboratory of Molecular Biology. The authors declare that they have no conflicts of interest with the contents of this article.

The atomic coordinates and structure factors (codes 5YTV, 5YTS, 5YTX, and 5YTT) have been deposited in the Protein Data Bank (<http://www.pdb.org/>).

<sup>1</sup> To whom correspondence may be addressed: Shanghai Institute of Biochemistry and Cell Biology, Chinese Academy of Sciences, Shanghai 200031, China. Tel.: 86-21-54921354; E-mail: [jyhui@sibcb.ac.cn](mailto:jyhui@sibcb.ac.cn).

<sup>2</sup> To whom correspondence may be addressed: Shanghai Institute of Biochemistry and Cell Biology, Chinese Academy of Sciences, Shanghai 200031, China. Tel.: 86-21-20778200; E-mail: [huangy@sibcb.ac.cn](mailto:huangy@sibcb.ac.cn).

<sup>3</sup> The abbreviations used are: CSD, cold shock domain; KH domain, K homology domain; STAR, a gene family involved in signal transduction and activation of RNA; FP, fluorescence polarization; SELEX, systematic evolution of ligands by exponential enrichment; FAM, fluorescein amidite; miRNA, microRNA; IP, immunoprecipitation; PDB, Protein Data Bank; oligo, oligomer.

YB-1 was found to be actively secreted, and serum YB-1 levels may be potentially utilized as a biomarker for cancer progression (25–28). Recent studies reported a role of YB-1 in sorting miRNAs and other small noncoding RNA species into exosomes (29, 30).

The YB-1 protein consists of a variable N-terminal Ala/Pro-rich domain (A/P), a central CSD, and a C-terminal domain (CTD), which is composed of basic and aromatic regions (Fig. 1A). The RNA-binding specificity of an RNA-binding protein is important for understanding its cellular functions and molecular mechanisms as well as for searching for its downstream targets. Early studies based on the *Xenopus* Y-box protein, FRGY2, suggest that the CSD in Y-box proteins is responsible for its specific interaction with RNA, whereas the Ala/Pro-rich domain and C-terminal domain stabilize its binding to RNA in a sequence-independent manner (31–33). The CSD of YB-1 adopts a classical OB-fold consisting of five anti-parallel  $\beta$ -strands to form a  $\beta$ -barrel (34). This  $\beta$ -barrel structure usually exists in nucleic acid-binding proteins carrying the ribonucleoprotein particle domain-1 and -2 (RNP-1 and RNP-2). In the previously reported CSD structures, CSDs only show limited sequence specificity, such as bacterial CspB and Lin28 (35, 36). However, how YB-1 CSD specifically recognizes its RNA-binding motif remains elusive.

In our previous studies, we showed that YB-1 specifically binds to a CA(U/C)C consensus sequence using the systematic evolution of ligands by exponential enrichment (SELEX) method (37). Mutational analyses showed that the second adenosine (A<sub>2</sub>) and the fourth cytidine (C<sub>4</sub>) in the CA(U/C)C consensus are critical for YB-1 recognition. YB-1 specifically recognizes the CAUC core motif in both *CD44* variable exon v5 and its upstream polypyrimidine region, which activates exon v5 inclusion by recruiting U2AF65 to the weak 3' splice site. Later, using the iCLIP-Seq method, we mapped the *in vivo* YB-1-binding sites at a genome-wide level and found that YB-1 preferentially recognizes a UYAUC motif, which closely resembles the binding motif determined by *in vitro* SELEX (38). In a recent study, the CAUC motif was also identified as a YB-1-binding motif in a fused cell line by photoactivatable ribonucleoside-enhanced cross-linking and immunoprecipitation (39). We also showed that YB-1 is up-regulated in glioblastoma and promotes cell proliferation by blocking the processing of miR-29b-2 via specific binding to the CAUC motif in the terminal loop region of pri-/pre-miR-29b-2 (38). These results demonstrate that the specific recognition of the YB-1-binding motif is crucial for its function.

To provide the structural basis for YB-1–RNA interactions, in this study, we resolved the high-resolution crystal structures of YB-1 CSD in complex with RNA-binding consensus sequence defined previously by using SELEX method (37). We also found that YB-1 CSD forms a homodimer both in crystal and in solution. Its dimerization is important for its RNA binding and function in splicing regulation. Taken together, our findings provide structural details and novel features of YB-1–RNA interactions.

## Results

### The CSD of YB-1 preferentially binds a single-stranded RNA oligomer

The CSD is located in the middle of YB-1 protein, spanning residues 50–130 (Fig. 1A). To investigate the binding affinities of YB-1 CSD to single-stranded or dsRNA oligos, we performed fluorescence polarization (FP) assays to measure the dissociation constants ( $K_D$ ). RNA oligomers used in the FP assays were designed to eliminate the secondary structures, including hairpin structure or more than four nucleotides of self-complementary sequence. In detail, RNA oligomers all contain a fluorescein amidite (FAM) group and six additional nucleotides (5'-gccaa-3') at the 5'-end and two nucleotides (5'-ua-3') at the 3'-end. The tetranucleotides in all sequence contexts are located in the middle. For convenience, we refer to 5'-FAM-gccaaUC<sub>1</sub>A<sub>2</sub>U<sub>3</sub>C<sub>4</sub>ua-3', which is derived from the high-affinity CA(U/C)C motif, as the WT sequence (f-rWT). The first cytidine shown as a capital letter in the sequence is position +1. The YB-1 CSD binds to f-rWT, with a  $K_D$  value of 1.26  $\mu$ M (Fig. 1B). However, no binding was detected for a dsRNA oligo, which was generated by annealing f-rWT with its complementary sequence. Therefore, our results indicate that the YB-1 CSD binds to single-stranded RNA oligomers rather than duplex RNAs.

### Overall structure of the YB-1 CSD in complex with a hexamer RNA

We then performed crystallization trials with the YB-1 CSD and a hexamer RNA, which is composed of the central CAUC motif (CAUC: 5'-U<sub>0</sub>C<sub>1</sub>A<sub>2</sub>U<sub>3</sub>C<sub>4</sub>U<sub>5</sub>-3'). We were able to grow crystals of the complex of YB-1 CSD–CAUC that diffracted to 1.7 Å in a space group of P6<sub>2</sub> (Table 1). The structure was solved by molecular replacement using the crystal structure of the *Bacillus subtilis* CspB CSD as a search model (PDB code 3PF5). The asymmetric unit is composed of one CSD bound to one RNA oligomer. The overall structure of the YB-1 CSD is a typical OB-fold, which is a closed  $\beta$ -barrel formed by five anti-parallel  $\beta$ -strands ( $\beta$ 1– $\beta$ 5) (Fig. 1C). The CAUC RNA oligomer bound on YB-1 CSD in an arc shape. U<sub>1</sub> and U<sub>6</sub> at each end of the RNA oligomer are missing in the electron density map; however, the CAUC consensus tetranucleotides are clearly visible (Fig. 1D). The CAUC RNA oligomer bound onto the surface of YB-1 CSD, which is formed by  $\beta$ 1– $\beta$ 3 with an interaction interface of 532.7 Å<sup>2</sup> (Fig. 1E), indicating the formation of a stable complex of YB-1 CSD with the CAUC RNA oligo. Moreover, the hydrophobic and partially basic surface of YB-1 CSD facilitated RNA binding.

### The YB-1 CSD interacts with RNA mainly through $\pi$ – $\pi$ stacking interactions, which are crucial for activating *CD44* exon v5 splicing

When bound to the YB-1 CSD, the CAUC RNA forms four  $\pi$ – $\pi$  stacking pairs with the pairing alignments of C<sub>1</sub>·His-87, A<sub>2</sub>·Phe-85, U<sub>3</sub>·Phe-74, and C<sub>4</sub>·Trp-65 (Fig. 2A). Sequence alignment showed that these four aromatic residues are highly conserved in cold shock proteins across species (Fig. 2B). To test the importance of these specific residues for the binding of the

## Crystal structure of YB-1–RNA complex

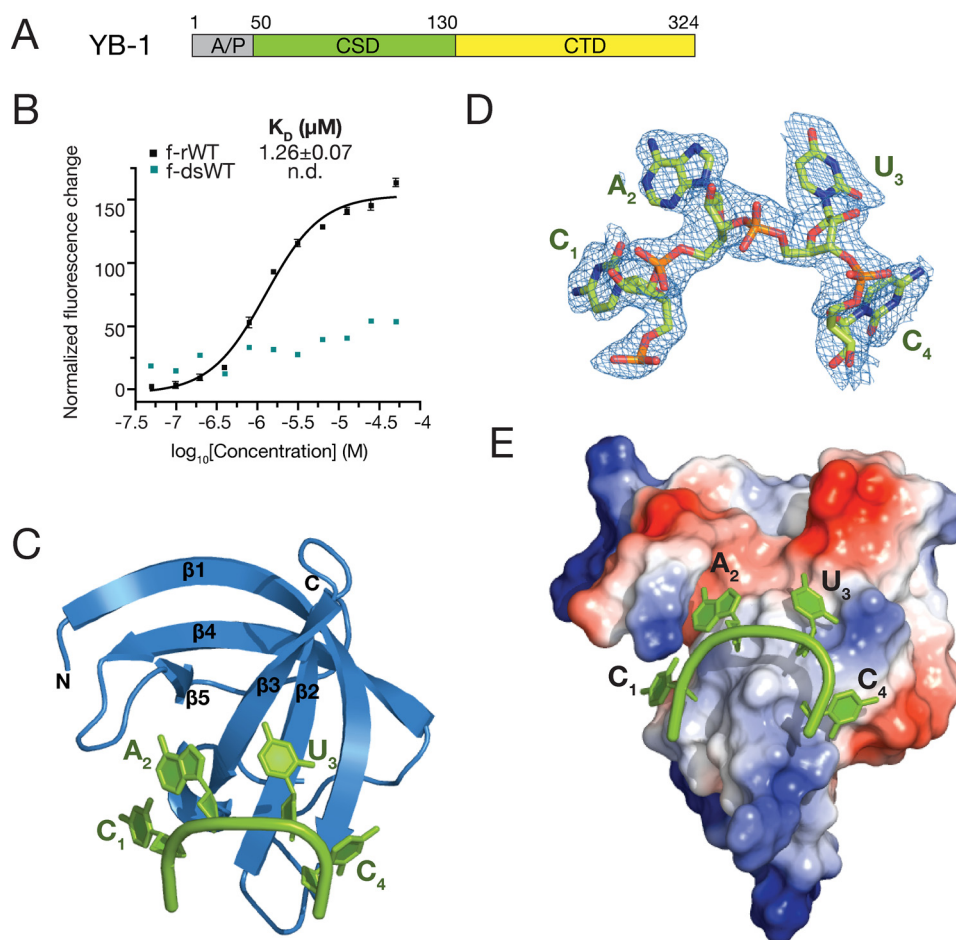


**Figure 1. Overall structure of YB-1 CSD in complex with CAUC.** *A*, schematic representation of the domain architecture of human YB-1. *B*, interactions between YB-1 CSD and fluorescently labeled f-rWT or f-dsRNA oligos were analyzed by fluorescence polarization. One nanomolar of fluorescently labeled RNA was incubated with the protein at different concentrations. Changes in the fluorescence intensity changes under polarized illumination were plotted. *Error bars*, S.D. ( $n = 3$ ). *C*, cartoon representation of the YB-1 CSD (blue) and CAUC (green) complex. YB-1 CSD represents a typical OB-fold, which is composed of five  $\beta$ -strands. *D*,  $2F_o - F_c$  electron density map (contoured at  $1.0 \sigma$  cutoff, blue mesh) of the tetranucleotide CAUC in the YB-1 CSD–CAUC structure. *E*, electrostatic potential surface analysis of the YB-1 CSD. RNA is bound to the hydrophobic and partially basic patch of the surface. *A/P*, Ala/Pro-rich domain; *CTD*, C-terminal domain.

CAUC RNA, we substituted the four residues His-87, Phe-85, Phe-74, and Trp-65 with Ala residues within the YB-1 CSD (H87A, F85A, F74A, and W65A, respectively). Each mutant abolished the binding to the RNA oligomer, suggesting that these residues are essential for RNA binding by the CSD of YB-1 (Fig. 2C).

We previously reported that YB-1 is necessary for the activation of *CD44* exon v5 splicing by binding to the CAUC elements in both exon v5 and its upstream intron (37). To test the impact of these key residues on splicing, we co-transfected full-length constructs expressing full-length WT YB-1 and its mutants carrying W65A, F74A, F85A, and H87A substitutions together with the *CD44* exon v5 minigene and analyzed exon v5 splicing by RT-PCR (Fig. 2, D and E). Each mutant exhibited a decrease in exon v5 inclusion compared with WT YB-1, whereas W65A or F74A showed stronger effects than F85A or H87A. The double mutation F85A/H87A resulted in a similar effect compared with each single mutation. Mutation of all four residues resulted in a significant decrease. Together, these results indicate that Trp-65 and Phe-74 play a major role in stimulating exon v5 splicing by YB-1.

### Sequence-specific recognition of the CAUC motif by YB-1 CSD

Structural analysis of the YB-1 CSD–CAUC complex revealed the underlying structure-based intermolecular interactions observed in the crystal structure of the complex, where a combination of specific hydrogen bonding, stacking, and hydrophobic interactions contributes to the anchoring of the RNA oligomer to the YB-1 CSD. The four nucleotides adopt *anti* conformations except for the  $A_2$  nucleotide, which is in *syn* conformation (Fig. 2A).

Besides the  $\pi$ – $\pi$  stacking interactions,  $C_1$  forms a network of intermolecular hydrogen bonds with Thr-89 and His-87 (Fig. 3A). The backbone of  $C_1$  is further stabilized by a water-mediated hydrogen bond with His-87, and its 2'-hydroxyl group on the sugar pucker forms hydrogen bonds with Lys-118. Lys-118 is involved in multiple interactions with the RNA oligomer. The side chain of Lys-118 not only forms a salt bridge and a hydrogen bond with the phosphate group of  $A_2$  (Fig. 3A), but stacks over  $A_2$  to buttress the cation– $\pi$ – $\pi$  sandwich structure. Moreover,  $N^6$  of  $A_2$  forms a hydrogen bond with the main chain of Lys-118.  $N^7$  of  $A_2$  comes to contact with Phe-85 via a water-

**Table 1**  
Crystallographic statistics of YB-1 CSD in complex with RNA oligos

	CAUC (5YTV)	A2U (5YTS)	U3A (5YTX)	C4G (5YTT)
<b>Data collection</b>				
Space group	P6 <sub>2</sub>	P6 <sub>2</sub>	P6 <sub>2</sub>	P6 <sub>2</sub>
Cell dimensions				
<i>a</i> , <i>b</i> , <i>c</i> (Å)	66.3, 66.3, 35.2	65.7, 65.7, 37.0	66.5, 66.5, 33.6	66.2, 66.2, 36.0
$\alpha$ , $\beta$ , $\gamma$ (degrees)	90, 90, 120	90, 90, 120	90, 90, 120	90, 90, 120
Resolution (Å)	30–1.70 (1.76–1.70) <sup>a</sup>	50–1.77 (1.83–1.77)	30–1.55 (1.61–1.55)	50–1.60 (1.66–1.60)
<i>R</i> <sub>merge</sub>	0.095 (0.327)	0.083 (0.600)	0.053 (0.609)	0.070 (0.671)
<i>I</i> / $\sigma$ ( <i>I</i> )	30.0 (6.8)	30.7 (1.9)	35.4 (2.2)	26.6 (2.4)
Completeness (%)	100.0 (100.0)	99.0 (94.1)	98.9 (98.9)	96.4 (78.5)
Redundancy	16.6 (12.3)	7.3 (5.3)	6.0 (5.0)	9.2 (6.9)
<b>Refinement</b>				
Resolution (Å)	30–1.7	30–1.77	30–1.55	30–1.60
No. of reflections	9,677	8,943	12,345	10,965
<i>R</i> <sub>work</sub> / <i>R</i> <sub>free</sub>	0.196/0.228	0.187/0.227	0.200/0.240	0.182/0.218
No. of atoms				
Protein	582	601	593	616
RNA	82	80	84	125
Water	52	57	50	62
Mean <i>B</i> -factors (Å <sup>2</sup> )				
Protein	25.4	28.4	32.1	21.5
RNA	41.6	44.5	60.2	47.5
Water	33.7	39.5	46.7	36.9
Root mean square deviations				
Bond lengths (Å)	0.007	0.006	0.006	0.007
Bond angles (degrees)	1.071	0.901	0.919	1.072
Ramachandran plot				
Favored (%)	100.0	94.7	100.0	100.0
Allowed (%)	0.0	5.3	0.0	0.0
Outlier (%)	0.0	0.0	0.0	0.0

<sup>a</sup> Numbers in parentheses are for the outer-resolution shell.

bridged hydrogen bond. In addition, the orientation of A<sub>2</sub> is further stabilized by its sugar phosphate backbone. A hydrogen bond between N<sup>3</sup> and O<sup>4'</sup> of A<sub>2</sub> was observed. Furthermore, in the crystal structure of YB-1 CSD–CAUC complex, N<sup>3</sup> and O<sup>2</sup> of U<sub>3</sub> form hydrogen bonds with the side chains of Asp-83 and Lys-64, respectively (Fig. 3B). A conserved salt bridge between Asp-83 and Lys-64 is formed to stabilize these two residues. Residues Trp-65, Asn-67, Asn-70, Tyr-72, and Asp-105 form key intermolecular contacts with C<sub>4</sub>. Additionally, the base of C<sub>4</sub> stacks on Trp-65 and contacts Trp-65, Asn-67, and Asp-105 via direct or water-mediated hydrogen bonds. The backbone sugar pucker of C<sub>4</sub> is shaped by Asn-70 and Tyr-72 by two hydrogen bond interactions.

#### Impact of YB-1 CSD mutants on *in vitro* binding affinity

To assess these interactions, site-specific mutagenesis as well as FP assays were performed (Fig. 3C). T89A, which is predicted to disrupt the hydrogen bond interactions with C<sub>1</sub>, decreased the binding affinity by about 4.3-fold, with a *K<sub>D</sub>* of 5.39 μM. Lys-118, which plays multiple roles in the recognition of A<sub>2</sub>, completely abolished the binding when mutated to Ala (Fig. 3C). Residues Asp-83 and Lys-64 directly interact with U<sub>3</sub>. Mutation of Asp-83 to Ala exhibits a *K<sub>D</sub>* of 3.10 μM, reflecting a 2.5-fold reduction in binding affinity compared with the WT, which is in contrast to the mutation of Lys-64, which dramatically decreased the binding; thus, Lys-64 plays a major role in the recognition of U<sub>3</sub> rather than Asp-83 (Fig. 3C). In addition, N67A, which disrupts the hydrogen bond between Asn-67 and the O<sup>2</sup> of C<sub>4</sub>, decreases the binding affinity by a factor of 4 (*K<sub>D</sub>* = 5.07 μM). In addition, there is a unique interaction between YB-1 CSD and the sugar-phosphate backbone of CAUC. The amide group of Asn-70 interacts with the 2'-hy-

droxyl group of the sugar ring of C<sub>4</sub> via a hydrogen bond. Asn-70 only exists in YB-1 CSD and not in bacterial Csp protein or mLin28 CSD (Fig. 2C). Mutation of Asn-70 to Ala decreased the binding by about 1.7-fold, with a *K<sub>D</sub>* of 2.19 ± 0.25 μM (Fig. 3C). Taken together, these residues play important roles in the specific recognition of the CAUC RNA oligomer by the YB-1 CSD.

#### Impact of complementary substitutions of the CAUC RNA oligo on binding to YB-1 CSD

To further investigate the molecular basis underlying sequence-specific recognition, we mutated each nucleotide on the CAUC motif to its complementary sequence and assessed the binding affinities. Mutation of C<sub>1</sub> to its complementary nucleotide guanine reduced the binding affinity by 1.8-fold, with a *K<sub>D</sub>* of 2.26 ± 0.06 μM (Fig. 4A). Similarly, the dissociation constant decreased by a factor of 2.2 (*K<sub>D</sub>* = 2.77 μM) for A2U, a factor of 1.1 (*K<sub>D</sub>* = 1.34 μM) for U3A, and a factor of 3.0 (*K<sub>D</sub>* = 3.77 μM) for C4G mutants (Fig. 4A), indicating that YB-1 CSD preferentially binds to the CAUC motif over its complementary mutants.

Next, we co-crystallized and determined the structures of YB-1 CSD in complex with RNA oligos carrying complementary mutations, including C1G (5'-U<sub>0</sub>G<sub>1</sub>A<sub>2</sub>U<sub>3</sub>C<sub>4</sub>U<sub>5</sub>-3'), A2U (5'-U<sub>0</sub>C<sub>1</sub>U<sub>2</sub>U<sub>3</sub>C<sub>4</sub>U<sub>5</sub>-3'), U3A (5'-U<sub>0</sub>C<sub>1</sub>A<sub>2</sub>A<sub>3</sub>C<sub>4</sub>U<sub>5</sub>-3'), and C4G (5'-U<sub>0</sub>C<sub>1</sub>A<sub>2</sub>U<sub>3</sub>G<sub>4</sub>U<sub>5</sub>-3'). Except for C1G, crystallization of YB-1 CSD with the other three mutant RNA oligomers was successful (Table 1), which allows us to obtain efficient information on the detailed interactions by comparing these protein–RNA complex structures. The binding mode of the four RNA oligos to YB-1 CSD is quite similar, with only a small conformational change at each nucleobase (Fig. 4, B–F).



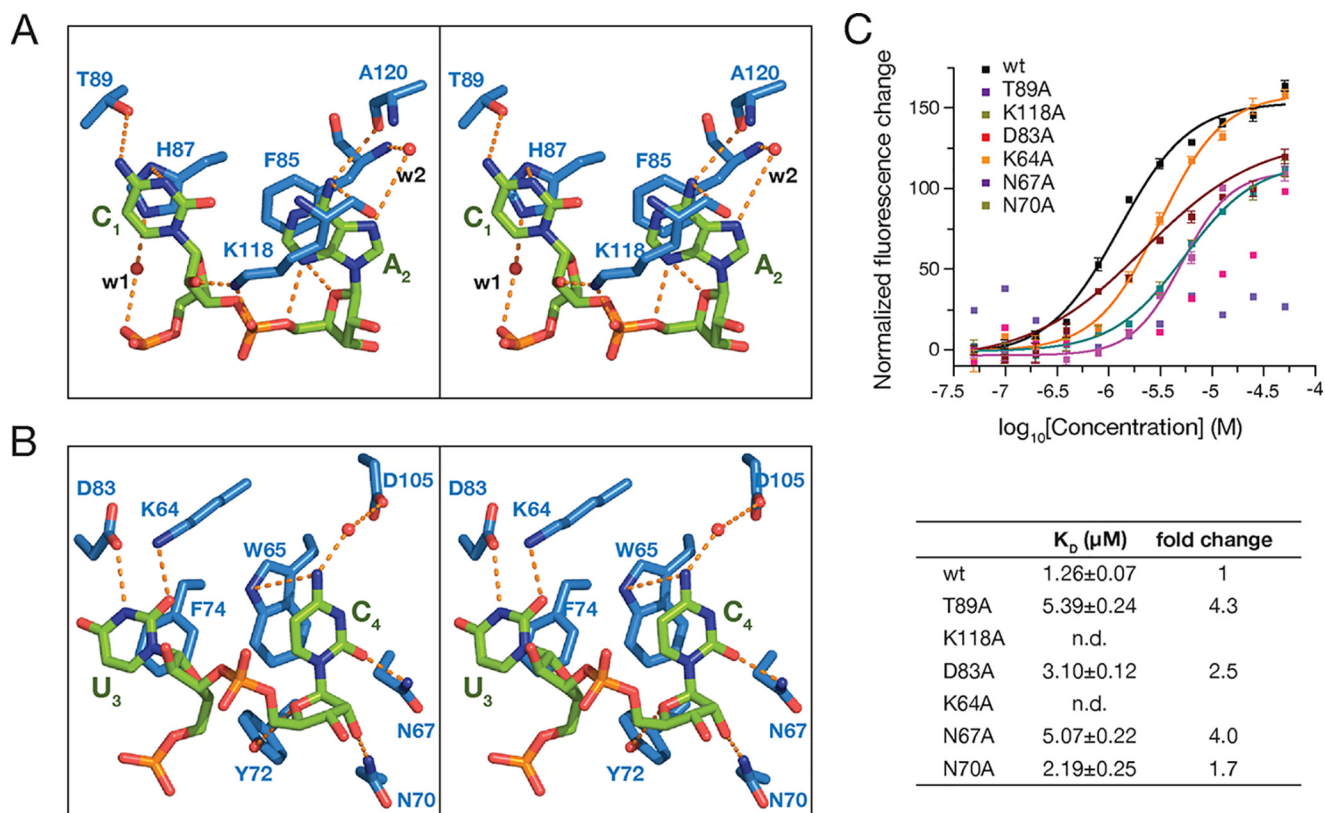


**Figure 3. Detailed interactions between the CAUC motif and YB-1 CSD.** *A*, stereo view of the recognition of  $C_1$  and  $A_2$ . *B*, stereo view of the recognition of  $U_3$  and  $C_4$ . *C*, mutation of the key residues involved in the interactions decreases the binding as measured by FP (top). Changes in fluorescence intensity under polarized illumination were plotted. The derived  $K_D$  is indicated. Error bars, S.D. ( $n = 3$ ). WT and mutant YB-1 CSD are indicated in the key. The dissociation constants ( $K_D$ ) are summarized in the table (bottom).

molecular interactions between  $A_2$  and its sugar phosphate backbone are also missing in the A2U complex structures. Similarly, in the crystal structure of YB-1 CSD–U3A,  $U_3$  is mutated to its complementary adenine. Thus, the amine group of Lys-64 is unable to form a hydrogen bond with  $C^4$  of  $A_3$  (Fig. 4H). Moreover,  $N^1$  of  $A_3$  could not form a hydrogen bond with Asp-83 due to the lack of hydrogen donors on  $N^1$ . According to the previous SELEX results, the third nucleotide in the core CAUC motif is flexible, and  $U_3$  could be cytosine. Mutation of  $U_3$  to adenine only shows mild impact on the binding affinity, suggesting the tolerance of different nucleotides in this position (Fig. 4I). Moreover, no hydrogen bond was observed between  $G_4$  and Asn-67 in the structure of YB-1 CSD–C4G complex, which is in contrast to the CAUC complex, where a hydrogen bond is formed between  $O^2$  of  $C_4$  and Asn-67. These findings further indicate that the YB-1 CSD has preference over the CAUC sequence.

#### YB-1 CSD forms a homodimer independent of RNA

Many RNA-binding proteins have a tendency to aggregate under low-salt conditions, with crowding agent, or upon binding to RNAs, which has been implicated in the aberrant formation of RNA granules in some diseases (40, 41). Full-length YB-1 can form a homomultimer, corresponding to  $\sim 440$  kDa, in a concentration-dependent manner (42). Moreover, the elution volume for CSD was smaller than expected on the size-exclusion chromatography. Therefore, it may be concluded that full-length YB-1, including the CSD, tends to oligomerize

in solution. In the crystal structures of YB-1 CSD and RNA complex, there is one molecule in an asymmetric unit. However, we observed intermolecular hydrogen bonds between symmetry-related YB-1 CSD molecules. YB-1 CSD exhibits as a homodimer (A–B) with a 2-fold axis. The area of the dimeric interface is  $489.0 \text{ \AA}^2$  (Fig. 5A). The carboxylate group of Asp-105 on molecule A interacts with the corresponding Asp-105' on molecule B, and this interaction is further stabilized by the main-chain amide group of Phe-66 and Phe-66' on each molecule (Fig. 5B). Moreover, Tyr-99 on molecule A forms a hydrogen bond with Glu-107' on molecule B. To exclude the possibility that dimerization of YB-1 CSD is due to crystal packing, we performed dynamic light scattering assays to monitor the molecular weight of YB-1 CSD in solution. A double mutant (DM) in which Tyr-99 and Asp-105 are substituted with Ala (Y99A/D105A) was generated to disrupt the intermolecular interactions. The result showed that the WT YB-1 CSD exhibited higher molecular weight than expected (Fig. 5C). As the protein concentration increased, no significant change in molecular weight was observed, which was similar to what was observed in a previous study, that YB-1 CSD behaves as a single peak on size-exclusion chromatography independent of protein concentration. Moreover, the elution profile of YB-1 CSD was earlier than expected, indicating that YB-1 CSD forms a stable multimer. In contrast, the DM exhibited a lower molecular weight that was approximately half of that

## Crystal structure of YB-1–RNA complex

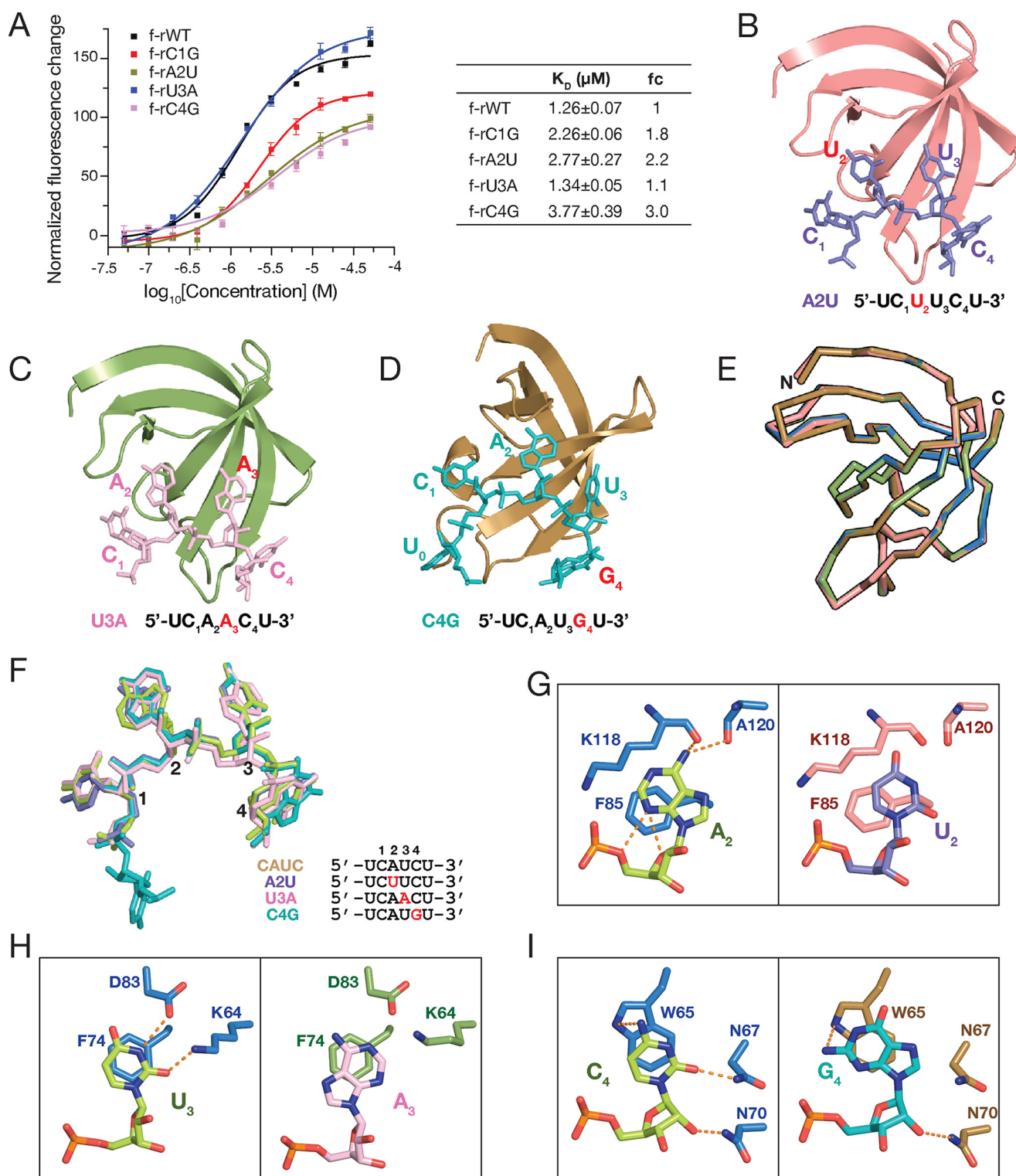


**Figure 4.** YB-1 CSD prefers to bind the CAUC motif. *A*,  $K_D$  of YB-1 CSD to CAUC motif and its complementary mutants as measured by FP (left). Changes in fluorescence intensity under polarized illumination were plotted. The derived  $K_D$  is indicated and summarized in the table (right). Error bars, S.D. ( $n = 3$ ). *B–D*, overall structures of YB-1 CSD in complex with A2U (purple; *B*), U3A (pink; *C*), and C4G (teal; *D*) RNA oligos. YB-1 CSD is shown in a cartoon representation. The RNA oligos are shown in stick mode. Sequences of the RNA oligos are listed below the structures. Mutated nucleotides are colored in red. *E*, superimposition of YB-1 CSDs shown in ribbons in the crystal structures of YB-1 CSD complexed with CAUC (blue), A2U (salmon), U3A (green), and C4G (brown). *F*, superimposition of the RNA oligos in the complex crystal structures. The color scheme is the same as in *B–D*. Mutated nucleotides are colored in red. *G–I*, detailed interactions between YB-1 CSD and the RNA oligos of the CAUC motif and its complementary sequences. *G*, comparison of the recognition of A<sub>2</sub> (left) and U<sub>2</sub> (right) in structures YB-1-CAUC and YB-1-A2U, respectively. *H*, comparison of the recognition of U<sub>3</sub> (left) and A<sub>3</sub> (right) in structures YB-1-CAUC and YB-1-U3A, respectively. *I*, comparison of the recognition of C<sub>4</sub> (left) and G<sub>4</sub> (right) in structures YB-1-CAUC and YB-1-C4G, respectively.

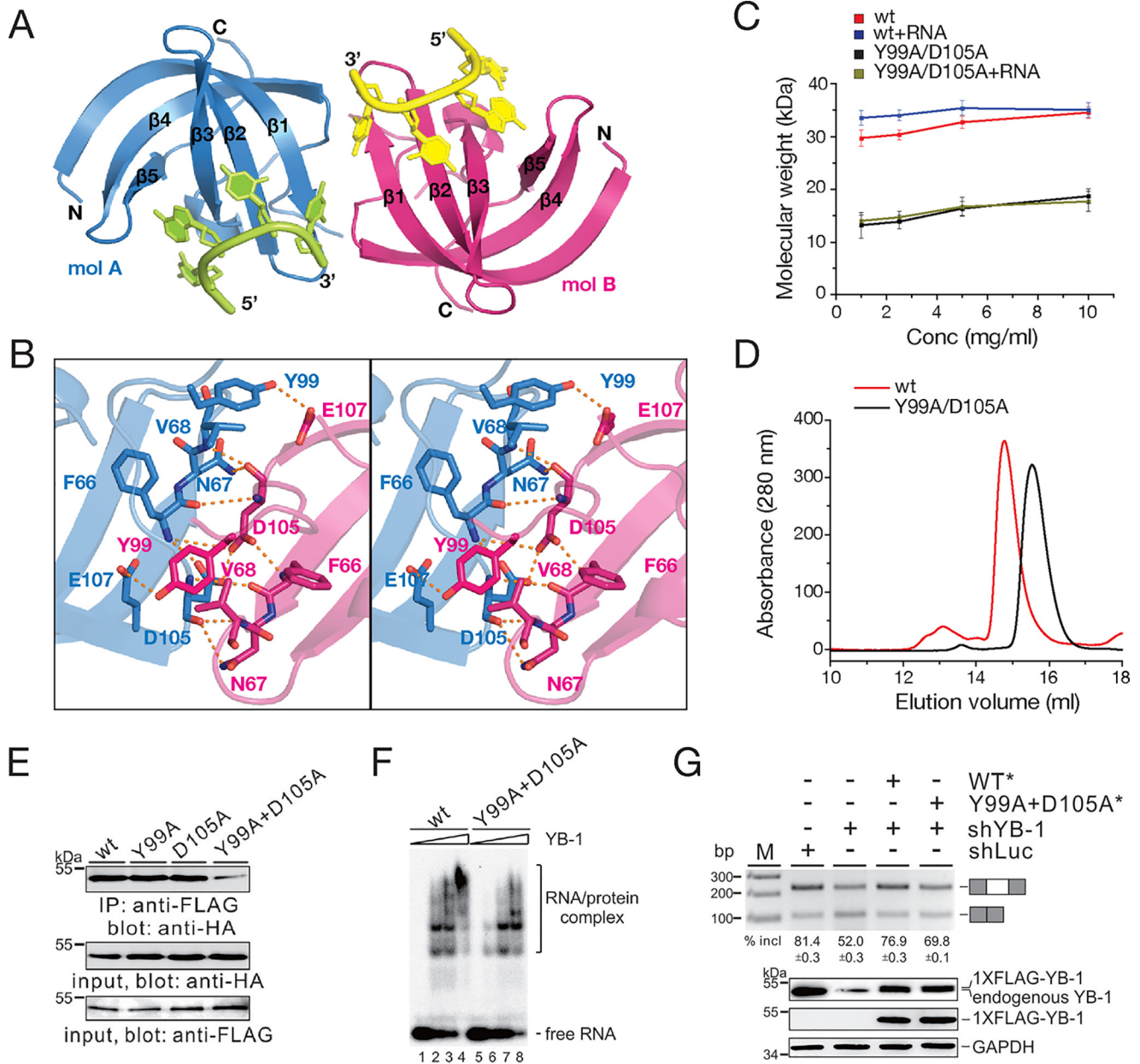


**Figure 5. Dimerization of YB-1 CSD.** *A*, cartoon representation of a YB-1 CSD dimer after symmetry-related operation. The two monomers are shown in blue (molecule A) and hot pink (molecule B). *B*, a stereo view showing the detailed interactions at the dimeric interface. *C*, molar mass of WT and mutant YB-1 CSD in the absence or presence of RNA oligo (5'-UCAUCU-3') at different concentrations as measured by dynamic light scattering. The color scheme is indicated. Error bars, S.D. ( $n = 3$ ). *D*, analytical size-exclusion chromatography profile of WT and mutant YB-1 CSD. The color scheme is indicated. *E*, co-IP of YB-1 WT and mutant proteins. The FLAG-tagged YB-1 expression construct was co-transfected with HA-tagged WT or mutant YB-1 into the HEK293 cells. Cell lysates were immunoprecipitated with an anti-FLAG antibody and immunoblotted with an anti-HA antibody. *F*, gel shift analysis of WT and DM YB-1-binding affinities to RNA derived from a *CD44* exon v5 minigene. Complexes were formed by incubating of  $^{32}\text{P}$ -labeled short RNAs with a 0-, 25-, 50-, and 100-fold molar excess of YB-1 CSD and separated on a 5% native gel. *G*, RT-PCR analysis of splicing activity of the pET-V5 minigene construct in MDA-MB-231 cells stably transfected with control shRNA or YB-1 shRNA or co-transfected with YB-1 shRNA together with resistant constructs expressing WT or mutant YB-1. The averages of exon inclusion percentage with S.D. values are shown below ( $n = 3$ ).

of the WT, supporting the notion that YB-1 CSD is likely to dimerize in solution. Interestingly, the oligomerization state was not affected by RNA binding, because both the WT and the DM showed a similar behavior in the dynamic light scattering assay in the presence or absence of RNA oligos. Moreover, we performed size-exclusion chromatography to check the oligomerization state of YB-1 CSD (Fig. 5D). WT YB-1 CSD was eluted in a volume earlier than the DM, thereby validating that YB-1 CSD exists as a dimer.

#### Abrogation of CSD dimerization leads to a reduction in RNA binding and splicing activation

To test the homodimer formation of YB-1 proteins *in vivo*, we performed co-immunoprecipitation (co-IP) experiments. The constructs expressing FLAG-tagged and HA-tagged full-length YB-1 were co-transfected into HEK293 cells. We observed that YB-1 is capable of interacting with itself in the presence of DNase and RNase (Fig. 5E, lane 1). Both mutants



## Crystal structure of YB-1–RNA complex

containing only one residue mutation (Y99A or D105A) still formed the homodimer (Fig. 5E, lanes 2 and 3); however, YB-1 DM (Y99A/D105A) exhibited a dramatic decrease in the interactions (Fig. 5E, lane 4). These data indicate that YB-1 CSD is oligomerized in solution, and residues Tyr-99 and Asp-105 are important for YB-1 oligomerization both *in vitro* and *in vivo*.

To address whether the function of YB-1 DM is different from that of the WT protein, we first conducted a gel shift experiment to test the RNA-binding activity of full-length YB-1 WT and DM using an RNA substrate derived from *CD44* exon v5 as reported previously (37). Compared to WT YB-1, the binding of YB-1 DM to RNA reduced (Fig. 5F). Next, to exclude the influence of endogenous YB-1, we performed *in vivo* splicing analysis of MDA-MB-231 cells after stable knockdown of YB-1. Consistent with previous results, knockdown of YB-1 inhibited exon v5 splicing. Expression of an shRNA-resistant YB-1 construct almost completely restored exon v5 inclusion, whereas the double mutant of YB-1 only partially restored exon v5 inclusion. Taken together, these results strongly suggest that the dimerization of the CSD is critical for YB-1–RNA interaction and its function in splicing regulation.

### Discussion

In this study, we determined the crystal structures of YB-1 CSD in complex with its core binding motif CAUC or several mutant RNA oligos at atomic resolution. A careful comparison of these structures revealed the detailed interactions between YB-1 CSD and RNA, thereby providing the mechanistic insights into the recognition of RNA by YB-1 in a sequence-dependent manner. We further show that YB-1 CSD forms a homodimer both in crystal and in solution. Mutations that disrupt the dimeric interface fail to form the homodimer of the CSD and result in a decrease in activating the inclusion of an alternative exon.

Comparison of structures of other members of the cold shock protein family (36, 43–45) indicated that YB-1 CSD is structurally similar to the CSD of mammalian Lin28 proteins (mouse Lin28a CSD, PDB code 3TS2; human Lin28a CSD, PDB code 5UDZ), which binds to pre-let-7 family RNAs (Fig. 6, A–C). Unlike bacterial Csp proteins, which preferentially bind to polythymidine DNA, the CSDs of YB-1 and hLin28 proteins favor binding RNAs. By comparing our structure with mammalian Lin28–RNA complex structures, the 3'-end of the RNA oligos exhibits different orientations. In our structures, the nucleobase of C<sub>4</sub> is stacking over the six-membered ring of the Trp-65 (Fig. 3B). The corresponding nucleotide takes different conformations either in the hLin28 CSD–RNA complex or in the mLin28 CSD–RNA complex (Fig. 6, D and E), suggesting a more flexible binding of the fourth nucleotide to Lin28 CSDs. This may be due to the hydrogen bond between Asn-70 and the 2'-OH of the sugar pucker of C<sub>4</sub> (Fig. 3B). Asn-70 is conserved in YB-1 proteins across species; however, it differs in Lin28 family proteins as well as in bacterial Csp proteins (Fig. 2B). In hLin28, the residue at the corresponding position is methionine, which is unable to form a hydrogen bond with the 2'-hydroxyl group. Moreover, the CSDs of YB-1 and hLin28 proteins function differently. Both proteins have multiple RNA-binding domains that play roles (37, 45). However, the sequence-specific binding of Lin28 proteins to single-stranded RNA is medi-

ated by the zinc-finger domain, and the CSD only shows limited sequence specificity (45, 46). In contrast, in YB-1, the CSD plays the central role in sequence-specific recognition (37).

In this work, we also found that the YB-1 CSD forms a homodimer both in crystal and in solution. We further showed that the dimerization influences the RNA-binding ability of the CSD. Dimerization of the RNA-binding protein has been reported previously, such as proteins containing the KH and STAR domains. For example, T-STAR and Sam68 function in alternative splicing through the dimerization of the KH domain, thus looping out regions to skip exons for pre-mRNA splicing (47). The RNA-binding element is therefore located on the opposite side of the KH dimer in an anti-parallel manner. In our structures, however, the two YB-1 dimer-bound RNA strands whose 3' termini are directed toward one another were in a loop conformation (Fig. 5A). This orientation seems to exclude the possibility that longer RNA strands bind onto the surface of the YB-1 dimer in a geometry resembling the crystal structure. However, a longer RNA strand may interact with the other molecule of YB-1 CSD, although we did not observe a direct interaction between them in the crystal structure. It is likely that the CSD dimerization facilitates the multimerization of the YB-1 protein and its RNA-binding ability. The full-length YB-1 protein was previously reported to form multimers on selected mRNAs, which leads to the inhibition of the translation of some mRNAs and disassembly of stress granules in neurons by competing with TDP-43 and FUS (40). In our study, we showed that the dimerization of YB-1 CSD synergizes the binding affinity to RNAs and regulates splicing *in vivo*. Therefore, we speculated that the homodimer formation of YB-1 CSD may contribute to the selection of target mRNAs and initiate aggregation onto RNAs. YB-1 is an oncogenic protein and highly expressed in various malignant tumors, making it a potential therapeutic target. Here, we showed that disruption of the CSD dimer interface impairs the alternative splicing of *CD44*. The newly identified dimerization interface of YB-1 CSD is a potential target site for novel drugs.

### Experimental procedures

#### Plasmid construction

A DNA fragment encoding the cold shock domain of human YB-1 (residues 50–130) was cloned into the pET28-SMT3 vector between the BamHI and Sall sites, which contains an N-terminal Ulp1-cleavable His<sub>6</sub>-SUMO tag. YB-1 mutants were generated by two-step PCR method and cloned into p3×Flag-CMV10-YB-1 plasmid (48) or pcDNA3-FLAG-YB-1. All constructs were sequence-verified.

#### Protein expression and purification

His<sub>6</sub>-SUMO-tagged recombinant proteins were expressed in *Escherichia coli* BL21 (DE3) under kanamycin selection. Cells were grown to an A<sub>600</sub> of 0.6, and protein expression was induced with 0.2 mM isopropyl-β-D-thiogalactopyranoside overnight at 18 °C. The cells were collected by centrifugation at 4,000 rpm for 15 min and were lysed by a French Press (JNBIO) at 4 °C. His<sub>6</sub>-SUMO-tagged proteins were purified by affinity chromatography using a HisTrap HP column (GE Healthcare), followed by the cleavage of the His<sub>6</sub>-SUMO tag using Ulp1 protease. The proteins were further purified by ion-exchange chro-

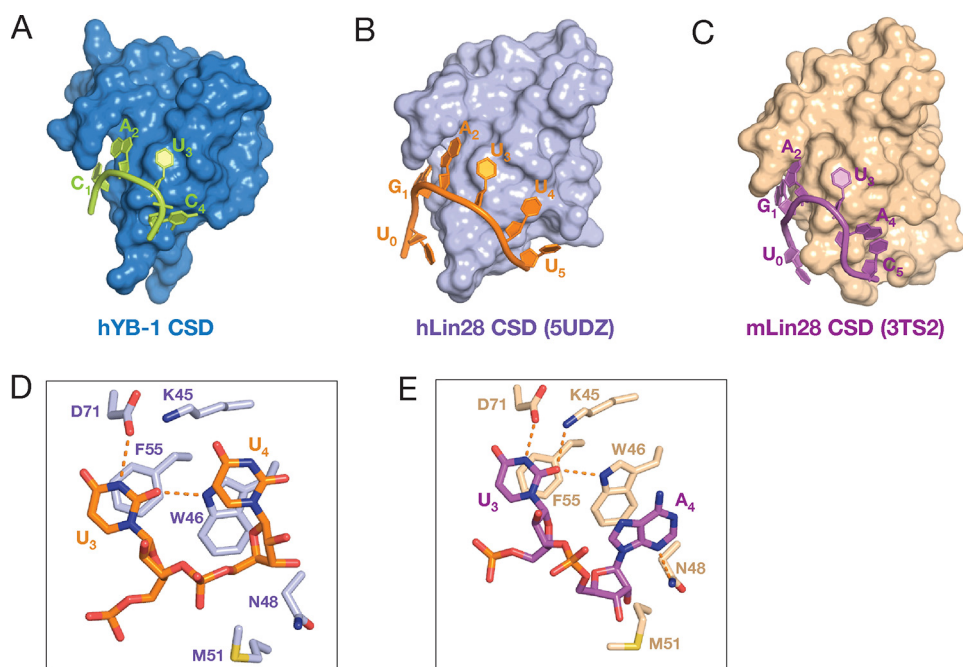


**Figure 6. Structural comparison of the cold shock domains.** A–C, surface representation of the CSD of YB-1 (blue; A), human Lin28a (light purple, PDB 5UDZ; B), and mouse Lin28a (wheat, PDB 3TS2; C) in complex with RNA oligos. Only the tetranucleotides with two adjacent nucleotides are shown. Sequences of the nucleotides are unified with the CAUC consensus sequence. RNA oligos are shown in *cartoon mode*. D, recognition of U<sub>3</sub> and U<sub>4</sub> of pre-let-7f by hLin28a CSD. U<sub>4</sub> stacks over the five-membered ring of the indole moiety. There is no hydrogen bond between Lys-45 and U<sub>3</sub> or between Asn-48 and U<sub>4</sub>. The corresponding Met-51 stands away from U<sub>4</sub>, and no hydrogen bond is formed between Met-51 and the 2'-OH of U<sub>4</sub>. E, recognition of U<sub>3</sub> and A<sub>4</sub> of pre-let-7g by mLin28 CSD. Asn-48 forms a hydrogen bond with the N<sup>3</sup> of A<sub>4</sub>. No hydrogen bond interaction exists between the 2'-OH of A<sub>4</sub> and Met-51.

matography using a HiTrap S column (GE Healthcare) and eluted in a gradient of NaCl. Size-exclusion chromatography was performed for the final purification of WT and mutant YB-1 CSD using Superdex G75 Hiload 16/60 column (GE Healthcare). Fractions containing target proteins were pooled and concentrated to 10 mg/ml in a buffer containing 10 mM Tris-Cl, pH 8.0, 100 mM NaCl, and 1 mM DTT.

#### Crystallization and structure determination

YB-1 CSD was mixed with RNA oligonucleotides (Bioneer) in a 1:2 ratio and incubated on ice for 1 h before crystallization. Crystals were grown at 17 °C by the hanging drop vapor diffusion method with the reservoir solution (0.1 M Hepes-HCl, pH 7.5, 2.0 M ammonium sulfate, and 5% isopropyl alcohol). Crystals of YB-1 CSD in complex with different RNA oligos were flash-frozen in liquid nitrogen. Diffraction data were collected at beamline BL17U1/BL19U1 of the Shanghai Synchrotron Radiation Facility (SSRF). The data set was processed using the HKL-2000 or HKL-3000 program (49). The structure was solved by molecular replacement using the structure of *B. subtilis* CspB (PDB code 3PF5) as a search model. Model building and structure refinement were carried out using COOT (50) and PHENIX (51). Buried surface area was calculated by PISA (52). All the of structural graphics were generated using PyMOL version 1.8 (Schrödinger, LLC, New York). The statistics of data collection and refinement were summarized in Table 1. The atomic coordinates and associated structure factors have been deposited in the Protein Data Bank under accession codes 5YTV, 5YTS, 5YTX, and 5YTT.

#### Fluorescence polarization assay

WT or mutant YB-1 CSD proteins were diluted using a buffer containing 20 mM Tris-HCl, pH 8.0, 100 mM NaCl, 1 mM DTT, 5%

glycerol to a series of concentrations, including 400, 200, 100, 50, 25, 12.5, 6.25, 3.125, 1.563, 0.781, and 0.391  $\mu$ M. The FAM-labeled RNA oligonucleotides were diluted in the same buffer to a final concentration of 1 nM. The final volume of each well in a 96-well plate (Corning) was brought to 100  $\mu$ l with the same buffer and incubated at room temperature in the dark for 30 min. The fluorescence polarization values were measured at an excitation wavelength of 485 nm and an emission wavelength of 528 nm using the Synergy Neo Multi-Mode Reader (Bio-Tek) at 25 °C. The normalized fluorescence change was quantitated using GEN 5, and the dissociation constant ( $K_D$ ) values were fitted and analyzed using the Dose Response function in OriginPro version 8.5.

#### Dynamic light scattering

All the samples used in dynamic light scattering experiments were centrifuged at 14,000 rpm for 10 min to remove large aggregates. The experiments were performed to measure average size of micelles using DynaPro Nanosta (Wyatt) operating at a wavelength of 658 nm at 4 °C. WT and mutant YB-1 CSD proteins were diluted in a buffer containing 10 mM Tris-HCl, pH 8.0, 100 mM NaCl, 0.1 mM DTT to a series of concentrations of 1.25, 2.5, 5, and 10 mg/ml. Each measurement was repeated three times to ensure reproducibility. The data were analyzed with OriginPro version 8.5.

#### Analytical size-exclusion chromatography

Analytical size-exclusion chromatography was performed for WT and mutant YB-1 CSD proteins using a Superdex 75 Increase 10/300 column (GE Healthcare) in a buffer containing 10 mM Tris-HCl, pH 8.0, 100 mM NaCl, and 1 mM DTT at a flow rate of 0.5 ml/min.

# Crystal structure of YB-1–RNA complex

## Gel shift assay

130 fmol of <sup>32</sup>P-labeled RNAs were incubated at 30 °C under standard splicing conditions with different molar excess of YB-1 proteins. A 5- $\mu$ l aliquot was removed and transferred to a new tube containing 1  $\mu$ l of tRNA (2 mg/ml). RNA–protein complexes were fractionated on a 5% native polyacrylamide gel.

## Co-IP

48 h after transfection, HEK293 cells were harvested and lysed in co-IP lysis buffer (50 mM Tris-HCl, pH 7.5, 150 mM KCl, 0.5% Nonidet P-40, 1 mM phenylmethylsulfonyl fluoride, 2  $\mu$ g/ml RNase A) at 4 °C for 15 min with rotating. The lysate was centrifuged at 13,000 rpm for 10 min at 4 °C. The supernatant was collected and incubated with 10  $\mu$ l of anti-FLAG M2 beads (Sigma) at 4 °C for 3 h with rotating. The beads were subsequently washed three times with 1 ml of co-IP washing buffer (50 mM Tris-HCl, pH 7.5, 500 mM KCl, 0.1% Nonidet P-40, 1 mM phenylmethylsulfonyl fluoride). The bound material was fractionated by SDS-PAGE followed by blotting with anti-HA antibody (Roche Applied Science).

## In vivo splicing

The day before transfection,  $3 \times 10^5$  MDA-MB-231 cells were seeded into a 3.5-cm culture dish. YB-1 expression plasmids and CD44 exon v5 minigene, pET-v5, were transfected using Lipofectamine 2000 (Invitrogen) according to the manufacturer's instructions. 48 h after cell transfection, total RNAs were isolated using TRIzol (Invitrogen). Total RNA (2.5  $\mu$ g) was annealed to oligo(dT)<sub>18</sub> and reverse-transcribed by Moloney murine leukemia virus (Promega) according to the manufacturer's instructions. The resulting first-strand cDNA was further amplified by PCR, using primers pET-for and pET-rev (37).

## Accession numbers

The coordinates for the structures reported in this paper have been deposited in the PDB under accession number 5YTV (YB-1 CSD–UCAUCU complex), 5YTS (YB-1 CSD–A2U complex), 5YTX (YB-1 CSD–U3A complex), and 5YTT (YB-1 CSD–C4G complex).

**Author contributions**—X.-J. Y. performed crystallization and solved the structures. H. Z., S.-R. M., and W.-J. W. performed *in vivo* splicing assays. X. Y., M. W., and Y. L. performed FP assays. J. H. and Y. H. conceived and supervised the project. J. H. and Y. H. wrote the manuscript.

**Acknowledgments**—We thank the staffs of the Large-scale Protein Preparation System at the National Facility for Protein Science in Shanghai (NFPS) and the staffs of beamlines BL17U1/BL19U1 at the Shanghai Synchrotron Radiation Facility (SSRF), Zhangjiang Laboratory, China, for providing technical support and assistance in data collection and analysis. We also thank Sandra E. Dunn (University of British Columbia) for providing the p3 $\times$ Flag-CMV10-YB-1 plasmid.

## References

1. Lyabin, D. N., Eliseeva, I. A., and Ovchinnikov, L. P. (2014) YB-1 protein: functions and regulation. *Wiley Interdiscip. Rev. RNA* **5**, 95–110 [CrossRef Medline](#)
2. Eliseeva, I. A., Kim, E. R., Guryanov, S. G., Ovchinnikov, L. P., and Lyabin, D. N. (2011) Y-box-binding protein 1 (YB-1) and its functions. *Biochemistry (Mosc.)* **76**, 1402–1433 [CrossRef Medline](#)
3. Didier, D. K., Schifffenbauer, J., Woulfe, S. L., Zacheis, M., and Schwartz, B. D. (1988) Characterization of the cDNA encoding a protein binding to the major histocompatibility complex class II Y box. *Proc. Natl. Acad. Sci. U.S.A.* **85**, 7322–7326 [CrossRef Medline](#)
4. Evdokimova, V. M., Wei, C. L., Sitikov, A. S., Simonenko, P. N., Lazarev, O. A., Vasilenko, K. S., Ustinov, V. A., Hershey, J. W., and Ovchinnikov, L. P. (1995) The major protein of messenger ribonucleoprotein particles in somatic cells is a member of the Y-box binding transcription factor family. *J. Biol. Chem.* **270**, 3186–3192 [CrossRef Medline](#)
5. Stickeler, E., Fraser, S. D., Honig, A., Chen, A. L., Berget, S. M., and Cooper, T. A. (2001) The RNA binding protein YB-1 binds A/C-rich exon enhancers and stimulates splicing of the CD44 alternative exon v4. *EMBO J.* **20**, 3821–3830 [CrossRef Medline](#)
6. Allemand, E., Hastings, M. L., Murray, M. V., Myers, M. P., and Krainer, A. R. (2007) Alternative splicing regulation by interaction of phosphatase PP2C $\gamma$  with nucleic acid-binding protein YB-1. *Nat. Struct. Mol. Biol.* **14**, 630–638 [CrossRef Medline](#)
7. Dutertre, M., Sanchez, G., De Cian, M. C., Barbier, J., Dardenne, E., Grataudou, L., Dujardin, G., Le Jossic-Corcors, C., Corcos, L., and Auboeuf, D. (2010) Cotranscriptional exon skipping in the genotoxic stress response. *Nat. Struct. Mol. Biol.* **17**, 1358–1366 [CrossRef Medline](#)
8. Chen, C. Y., Gherzi, R., Andersen, J. S., Gaietta, G., Jürchott, K., Royer, H. D., Mann, M., and Karin, M. (2000) Nucleolin and YB-1 are required for JNK-mediated interleukin-2 mRNA stabilization during T-cell activation. *Genes Dev.* **14**, 1236–1248 [Medline](#)
9. Evdokimova, V., Ruzanov, P., Imataka, H., Raught, B., Svitkin, Y., Ovchinnikov, L. P., and Sonenberg, N. (2001) The major mRNA-associated protein YB-1 is a potent 5' cap-dependent mRNA stabilizer. *EMBO J.* **20**, 5491–5502 [CrossRef Medline](#)
10. van Zalen, S., Jeschke, G. R., Hexner, E. O., and Russell, J. E. (2012) AUF-1 and YB-1 are critical determinants of  $\beta$ -globin mRNA expression in erythroid cells. *Blood* **119**, 1045–1053 [CrossRef Medline](#)
11. Nekrasov, M. P., Ivshina, M. P., Chernov, K. G., Kovrigina, E. A., Evdokimova, V. M., Thomas, A. A., Hershey, J. W., and Ovchinnikov, L. P. (2003) The mRNA-binding protein YB-1 (p50) prevents association of the eukaryotic initiation factor eIF4G with mRNA and inhibits protein synthesis at the initiation stage. *J. Biol. Chem.* **278**, 13936–13943 [CrossRef Medline](#)
12. Svitkin, Y. V., Evdokimova, V. M., Brasey, A., Pestova, T. V., Fantus, D., Yanagiya, A., Imataka, H., Skabkin, M. A., Ovchinnikov, L. P., Merrick W. C., and Sonenberg, N. (2009) General RNA-binding proteins have a function in poly(A)-binding protein-dependent translation. *EMBO J.* **28**, 58–68 [CrossRef Medline](#)
13. Lindquist, J. A., and Mertens, P. R. (2018) Cold shock proteins: from cellular mechanisms to pathophysiology and disease. *Cell Commun. Signal.* **16**, 63 [CrossRef Medline](#)
14. Bergmann, S., Royer-Pokora, B., Fietze, E., Jürchott, K., Hildebrandt, B., Trost, D., Leenders, F., Claude, J. C., Theuring, F., Bargou, R., Dietel, M., and Royer, H. D. (2005) YB-1 provokes breast cancer through the induction of chromosomal instability that emerges from mitotic failure and centrosome amplification. *Cancer Res.* **65**, 4078–4087 [CrossRef Medline](#)
15. Kosnopfel, C., Sinnberg, T., and Schitteck, B. (2014) Y-box binding protein 1—a prognostic marker and target in tumour therapy. *Eur. J. Cell Biol.* **93**, 61–70 [CrossRef Medline](#)
16. Maurya, P. K., Mishra, A., Yadav, B. S., Singh, S., Kumar, P., Chaudhary, A., Srivastava, S., Murugesan, S. N., and Mani, A. (2017) Role of Y box protein-1 in cancer: as potential biomarker and novel therapeutic target. *J. Cancer* **8**, 1900–1907 [CrossRef Medline](#)
17. Ohga, T., Uchiyumi, T., Makino, Y., Koike, K., Wada, M., Kuwano, M., and Kohno, K. (1998) Direct involvement of the Y-box binding protein YB-1 in genotoxic stress-induced activation of the human multidrug resistance 1 gene. *J. Biol. Chem.* **273**, 5997–6000 [CrossRef Medline](#)
18. Jürchott, K., Bergmann, S., Stein, U., Walther, W., Janz, M., Manni, L., Piaggio, G., Fietze, E., Dietel, M., and Royer, H. D. (2003) YB-1 as a cell cycle-regulated transcription factor facilitating cyclin A and cyclin B1 gene expression. *J. Biol. Chem.* **278**, 27988–27996 [CrossRef Medline](#)

19. Wu, J., Lee, C., Yokom, D., Jiang, H., Cheang, M. C., Yorida, E., Turbin, D., Berquin, I. M., Mertens, P. R., Iftner, T., Gilks, C. B., and Dunn, S. E. (2006) Disruption of the Y-box binding protein-1 results in suppression of the epidermal growth factor receptor and HER-2. *Cancer Res.* **66**, 4872–4879 [CrossRef Medline](#)
20. Astanehe, A., Finkbeiner, M. R., Hojabrpour, P., To, K., Fotovati, A., Shadeo, A., Stratford, A. L., Lam, W. L., Berquin, I. M., Duronio V., and Dunn, S. E. (2009) The transcriptional induction of PIK3CA in tumor cells is dependent on the oncoprotein Y-box binding protein-1. *Oncogene* **28**, 2406–2418 [CrossRef Medline](#)
21. Finkbeiner, M. R., Astanehe, A., To, K., Fotovati, A., Davies, A. H., Zhao, Y., Jiang, H., Stratford, A. L., Shadeo, A., Boccaccio, C., Comoglio, P., Mertens, P. R., Eirew, P., Raouf, A., Eaves, C. J., and Dunn, S. E. (2009) Profiling YB-1 target genes uncovers a new mechanism for MET receptor regulation in normal and malignant human mammary cells. *Oncogene* **28**, 1421–1431 [CrossRef Medline](#)
22. To, K., Fotovati, A., Reipas, K. M., Law, J. H., Hu, K., Wang, J., Astanehe, A., Davies, A. H., Lee, L., Stratford, A. L., Raouf, A., Johnson, P., Berquin, I. M., Royer, H. D., Eaves, C. J., and Dunn, S. E. (2010) Y-box binding protein-1 induces the expression of CD44 and CD49f leading to enhanced self-renewal, mammosphere growth, and drug resistance. *Cancer Res.* **70**, 2840–2851 [CrossRef Medline](#)
23. Evdokimova, V., Tognon, C., Ng, T., Ruzanov, P., Melnyk, N., Fink, D., Sorokin, A., Ovchinnikov, L. P., Davicioni, E., Triche, T. J., and Sorensen, P. H. (2009) Translational activation of snail1 and other developmentally regulated transcription factors by YB-1 promotes an epithelial-mesenchymal transition. *Cancer Cell* **15**, 402–415 [CrossRef Medline](#)
24. El-Naggar, A. M., Veinotte, C. J., Cheng, H., Grunewald, T. G., Negri, G. L., Somasekharan, S. P., Corkery, D. P., Tirode, F., Mathers, J., Khan, D., Kyle, A. H., Baker, J. H., LePard, N. E., McKinney, S., Hajee, S., *et al.* (2015) Translational activation of HIF1 $\alpha$  by YB-1 promotes sarcoma metastasis. *Cancer Cell* **27**, 682–697 [CrossRef Medline](#)
25. Frye, B. C., Halfter, S., Djurdjaj, S., Muehlenberg, P., Weber, S., Raffetseder, U., En-Nia, A., Knott, H., Baron, J. M., Dooley, S., Bernhagen, J., and Mertens, P. R. (2009) Y-box protein-1 is actively secreted through a non-classical pathway and acts as an extracellular mitogen. *EMBO Rep.* **10**, 783–789 [CrossRef Medline](#)
26. Rauen, T., Raffetseder, U., Frye, B. C., Djurdjaj, S., Muehlenberg, P. J., Eitner, F., Lendahl, U., Bernhagen, J., Dooley, S., and Mertens, P. R. (2009) YB-1 acts as a ligand for Notch-3 receptors and modulates receptor activation. *J. Biol. Chem.* **284**, 26928–26940 [CrossRef Medline](#)
27. Rohr, I., Braicu, E. I., En-Nia, A., Heinrich, M., Richter, R., Chekerov, R., Dechend, R., Heidecke, H., Dragun, D., Schäfer, R., Gorny, X., Lindquist, J. A., Brandt, S., Sehouli, J., and Mertens, P. R. (2016) Y-box protein-1/p18 as novel serum marker for ovarian cancer diagnosis: a study by the Tumor Bank Ovarian Cancer (TOC). *Cytokine* **85**, 157–164 [CrossRef Medline](#)
28. Ferreira, A. R., Bettencourt, M., Alho, I., Costa, A. L., Sousa, A. R., Mansinho, A., Abreu, C., Pulido, C., Macedo, D., Vendrell, I., Pacheco, T. R., Costa, L., and Casimiro, S. (2017) Serum YB-1 (Y-box binding protein 1) as a biomarker of bone disease progression in patients with breast cancer and bone metastases. *J. Bone Oncol.* **6**, 16–21 [CrossRef Medline](#)
29. Shurtleff, M. J., Temoche-Diaz, M. M., Karfilis, K. V., Ri, S., and Schekman, R. (2016) Y-box protein 1 is required to sort microRNAs into exosomes in cells and in a cell-free reaction. *Elife* **5**, e19276 [CrossRef Medline](#)
30. Shurtleff, M. J., Yao, J., Qin, Y., Nottingham, R. M., Temoche-Diaz, M. M., Schekman, R., and Lambowitz, A. M. (2017) Broad role for YBX1 in defining the small noncoding RNA composition of exosomes. *Proc. Natl. Acad. Sci. U.S.A.* **114**, E8987–E8995 [CrossRef Medline](#)
31. Manival, X., Ghisolfi-Nieto, L., Joseph, G., Bouvet, P., and Erard, M. (2001) RNA-binding strategies common to cold-shock domain- and RNA recognition motif-containing proteins. *Nucleic Acids Res.* **29**, 2223–2233 [CrossRef Medline](#)
32. Bouvet, P., Matsumoto, K., and Wolffe, A. P. (1995) Sequence-specific RNA recognition by the Xenopus Y-box proteins: an essential role for the cold shock domain. *J. Biol. Chem.* **270**, 28297–28303 [CrossRef Medline](#)
33. Matsumoto, K., Meric, F., and Wolffe, A. P. (1996) Translational repression dependent on the interaction of the Xenopus Y-box protein FRGY2 with mRNA: role of the cold shock domain, tail domain, and selective RNA sequence recognition. *J. Biol. Chem.* **271**, 22706–22712 [CrossRef Medline](#)
34. Kloks, C. P., Spronk, C. A., Lasonder, E., Hoffmann, A., Vuister, G. W., Grzesiek, S., and Hilbers, C. W. (2002) The solution structure and DNA-binding properties of the cold-shock domain of the human Y-box protein YB-1. *J. Mol. Biol.* **316**, 317–326 [CrossRef Medline](#)
35. Max, K. E., Zeeb, M., Bienert, R., Balbach, J., and Heinemann, U. (2006) T-rich DNA single strands bind to a preformed site on the bacterial cold shock protein Bs-CspB. *J. Mol. Biol.* **360**, 702–714 [CrossRef Medline](#)
36. Mayr, F., Schütz, A., Döge, N., and Heinemann, U. (2012) The Lin28 cold-shock domain remodels pre-let-7 microRNA. *Nucleic Acids Res.* **40**, 7492–7506 [CrossRef Medline](#)
37. Wei, W. J., Mu, S. R., Heiner, M., Fu, X., Cao, L. J., Gong, X. F., Bindereif, A., and Hui, J. (2012) YB-1 binds to CAUC motifs and stimulates exon inclusion by enhancing the recruitment of U2AF to weak polypyrimidine tracts. *Nucleic Acids Res.* **40**, 8622–8636 [CrossRef Medline](#)
38. Wu, S. L., Fu, X., Huang, J., Jia, T. T., Zong, F. Y., Mu, S. R., Zhu, H., Yan, Y., Qiu, S., Wu, Q., Yan, W., Peng, Y., Chen, J., and Hui, J. (2015) Genome-wide analysis of YB-1-RNA interactions reveals a novel role of YB-1 in miRNA processing in glioblastoma multiforme. *Nucleic Acids Res.* **43**, 8516–8528 [CrossRef Medline](#)
39. Hinze, F., Drewe-Boss, P., Milek, M., Ohler, U., Landthaler, M., and Gotthardt, M. (2018) Expanding the map of protein-RNA interaction sites via cell fusion followed by PAR-CLIP. *RNA Biol.* **15**, 359–368 [CrossRef Medline](#)
40. Harrison, A. F., and Shorter, J. (2017) RNA-binding proteins with prion-like domains in health and disease. *Biochem. J.* **474**, 1417–1438 [CrossRef Medline](#)
41. Abrakhi, S., Kretov, D. A., Desforgues, B., Dobra, I., Bouhss, A., Pastré, D., and Hamon, L. (2017) Nanoscale analysis reveals the maturation of neurodegeneration-associated protein aggregates: grown in mRNA granules then released by stress granule proteins. *ACS Nano* **11**, 7189–7200 [CrossRef Medline](#)
42. Guryanov, S. G., Filimonov, V. V., Timchenko, A. A., Melnik, B. S., Kihara, H., Kutyschenko, V. P., Ovchinnikov, L. P., and Semisotnov, G. V. (2013) The major mRNA protein YB-1: structural and association properties in solution. *Biochim. Biophys. Acta* **1834**, 559–567 [CrossRef Medline](#)
43. Max, K. E., Zeeb, M., Bienert, R., Balbach, J., and Heinemann, U. (2007) Common mode of DNA binding to cold shock domains: crystal structure of hexathymidine bound to the domain-swapped form of a major cold shock protein from *Bacillus caldolyticus*. *FEBS J.* **274**, 1265–1279 [CrossRef Medline](#)
44. Sachs, R., Max, K. E., Heinemann, U., and Balbach, J. (2012) RNA single strands bind to a conserved surface of the major cold shock protein in crystals and solution. *RNA* **18**, 65–76 [CrossRef Medline](#)
45. Nam, Y., Chen, C., Gregory, R. I., Chou, J. J., and Sliz, P. (2011) Molecular basis for interaction of let-7 microRNAs with Lin28. *Cell* **147**, 1080–1091 [CrossRef Medline](#)
46. Loughlin, F. E., Gebert, L. F., Towbin, H., Brunschweiler, A., Hall, J., and Allain, F. H. (2011) Structural basis of pre-let-7 miRNA recognition by the zinc knuckles of pluripotency factor Lin28. *Nat. Struct. Mol. Biol.* **19**, 84–89 [CrossRef Medline](#)
47. Feracci, M., Foot, J. N., Grellescheid, S. N., Danilenko, M., Stehle, R., Gonchar, O., Kang, H. S., Dalgliesh, C., Meyer, N. H., Liu, Y., Lahat, A., Sattler, M., Eperon, I. C., Elliott, D. J., and Dominguez, C. (2016) Structural basis of RNA recognition and dimerization by the STAR proteins T-STAR and Sam68. *Nat. Commun.* **7**, 10355 [CrossRef Medline](#)
48. Sutherland, B. W., Kucab, J., Wu, J., Lee, C., Cheang, M. C., Yorida, E., Turbin, D., Dedhar, S., Nelson, C., Pollak, M., Leighton Grimes, H., Miller, K., Badve, S., Huntsman, D., Blake-Gilks, C., *et al.* (2005) Akt phosphorylates the Y-box binding protein 1 at Ser102 located in the cold shock domain and affects the anchorage-independent growth of breast cancer cells. *Oncogene* **24**, 4281–4292 [CrossRef Medline](#)
49. Otwinowski, Z., and Minor, W. (1997) Processing of X-ray diffraction data collected in oscillation mode. *Methods Enzymol.* **276**, 307–326 [CrossRef Medline](#)

## Crystal structure of YB-1–RNA complex

50. Emsley, P., and Cowtan, K. (2004) Coot: model-building tools for molecular graphics. *Acta Crystallogr. D Biol. Crystallogr.* **60**, 2126–2132 [CrossRef](#) [Medline](#)
51. Adams, P. D., Afonine, P. V., Bunkóczi, G., Chen, V. B., Davis, I. W., Echols, N., Headd, J. J., Hung, L. W., Kapral, G. J., Grosse-Kunstleve, R. W., McCoy, A. J., Moriarty, N. W., Oeffner, R., Read, R. J., Richardson, D. C., *et al.* (2010) PHENIX: a comprehensive Python-based system for macromolecular structure solution. *Acta Crystallogr. D Biol. Crystallogr.* **66**, 213–221 [CrossRef](#) [Medline](#)
52. Krissinel, E., and Henrick, K. (2007) Inference of macromolecular assemblies from crystalline state. *J. Mol. Biol.* **372**, 774–797 [CrossRef](#) [Medline](#)